International Journal of Thermophysics, Vol. 21, No. 3, 2000

Thermodynamic Properties of Sulfur Hexafluoride

J. J. Hurly,[1,2] D. R. Defibaugh,[1] and M. R. Moldover[1]

Received September 15, 1999

We present new vapor phase speed-of-sound data $u(P, T)$, new Burnett density–pressure–temperature data $\rho(P, T)$, and a few vapor pressure measurements for sulfur hexafluoride (SF_6). The speed-of-sound data spanned the temperature range $230\ K \leqslant T \leqslant 460\ K$ and reached maximum pressures that were the lesser of 1.5 MPa or 80% of the vapor pressure of SF_6. The Burnett $\rho(P, T)$ data were obtained on isochores spanning the density range $137\ mol \cdot m^{-3} \leqslant \rho \leqslant 4380\ mol \cdot m^{-3}$ and the temperature range $283\ K \leqslant T \leqslant 393\ K$. (The corresponding pressure range is $0.3\ MPa \leqslant P \leqslant 9.0\ MPa$.) The $u(P, T)$ data below 1.5 MPa were correlated using a model hard-core, Lennard–Jones intermolecular potential for the second and third virial coefficients and a polynomial for the perfect gas heat capacity. The resulting equation of state has very high accuracy at low densities; it is useful for calibrating mass flow controllers and may be extrapolated to 1000 K. The new $u(P, T)$ data and the new $\rho(P, T)$ data were simultaneously correlated with a virial equation of state containing four terms with the temperature dependences of model square-well potentials. This correlation extends nearly to the critical density and may help resolve contradictions among data sets from the literature.

KEY WORDS: Burnett measurements; equation of state; heat capacity; intermolecular potential; speed of sound; sulfur hexafluoride; SF_6; thermodynamic properties; vapor pressure; virial coefficients.

1. INTRODUCTION

Sulfur hexafluoride (SF_6) is chemically and thermally stable and it is strongly electronegative. For these and other reasons, it is widely used at pressures of several bar as an insulator for high-voltage equipment. The

[1] Physical and Chemical Properties Division, Chemical Science and Technology Laboratory, National Institute of Standards and Technology, Gaithersburg, Maryland 20899-8380, U.S.A.

[2] To whom correspondence should be addressed.

0195-928X/00/0500-0739$18.00/0

present study of SF_6 was stimulated by its use in the semiconductor processing industry as a surrogate gas for calibrating mass flow controllers. In this application, heat transfer by gaseous SF_6 must be well understood at temperatures from 20 to 150°C near ambient pressure. Thus, accurate data are required for the constant pressure, ideal-gas heat capacity C_P^0, virial coefficients, and viscosity and thermal conductivity. Here, we provide the data for C_P^0 and the virial coefficients. Because SF_6 is a nearly spherical, polyatomic molecule, its effective pair potential has been modeled frequently [1, 2]. The present data can be used to parametrize such models.

Several equations of state have been proposed for SF_6. In 1983, Oda et al. [3] reviewed the published data and developed an equation of state valid from 222 to 500 K and at pressures up to 50 MPa. In 1990, Cole and de Reuck [4] presented an "interim equation of state" in the form of a reduced Helmholtz energy function. Cole and de Reuck's work incorporated results published after 1983 and included pseudo-data generated from the theory of corresponding states. Their Helmholtz function represented the thermodynamic properties of SF_6 in the temperature range from 222.38 to 525 K and at pressures up to 55 MPa. Cole and de Reuck referred to their equation of state as "interim" because they were unable definitively to resolve inconsistencies in the published data that they used. The present work may resolve some of the inconsistencies identified by Cole and de Reuck.

Here, we report speed-of-sound $u(P, T)$ measurements made with an acoustic resonator and density–pressure–temperature $\rho(P, T)$ measurements made with a Burnett apparatus. Figure 1 displays the location of these data relative to the vapor pressure of SF_6. The speed of sound was measured as a function of the pressure on 15 isotherms spanning the temperature range $230\ \mathrm{K} \leqslant T \leqslant 460\ \mathrm{K}$. The maximum pressures were the lesser of 1.5 MPa or 80% of the vapor pressure of SF_6. The corresponding densities are in the range from $21.6\ \mathrm{mol \cdot m^{-3}} \leqslant \rho \leqslant 661.0\ \mathrm{mol \cdot m^{-3}}$. The Burnett $\rho(P, T)$ data were obtained on isochores spanning the density range $137\ \mathrm{mol \cdot m^{-3}} \leqslant \rho \leqslant 4380\ \mathrm{mol \cdot m^{-3}}$ and the temperature range $283\ \mathrm{K} \leqslant T \leqslant 393\ \mathrm{K}$. (The corresponding pressure range is $0.3\ \mathrm{MPa} \leqslant P \leqslant 9.0\ \mathrm{MPa}$.)

The speed-of-sound data $u(P, T)$ were first analyzed to obtain $C_P^0(T)$, the constant-pressure, perfect-gas, molar heat capacity. To do so, the data on each isotherm were fitted by a polynomial function of the pressure to obtain the zero-pressure intercept $u(0, T)$ from which we obtained $C_P^0(T)$ using the relation $C_P^0(T) = R/(1 - RT/[Mu(0, T)])$, where M is the molar mass of SF_6 and $R = 8.314471\ \mathrm{J \cdot K^{-1}\ mol^{-1}}$ is the universal gas constant. Then, we represented $C_P^0(T)$ by a polynomial function of the temperature. Finally, the entire $u(P, T)$ data set was fitted by a virial equation of state to obtain the second and third density virial coefficients $B(T)$ and $C(T)$.

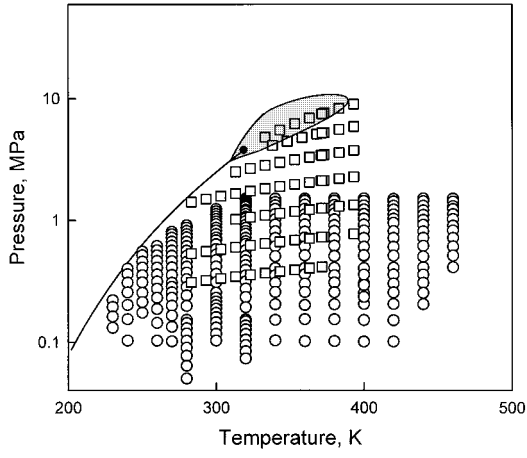

Fig. 1. States in pressure–temperature space covered by our experimental measurements: (○) speed-of-sound measurements; (□) Burnett density measurements. The vapor pressure curve is shown. The shaded region surrounding the critical point indicates the region in which the equation of state of Wyczalkowska and Sengers [34] is valid.

For this fit, only four parameters were adjusted. These four parameters appeared in the hard-core Lennard–Jones (HCLJ) intermolecular potential and in a related three-body term. The potential was integrated to compute both $B(T)$ and $C(T)$. The four-parameter HCLJ virial equation of state is very accurate throughout the range of the $u(P, T)$ data; thus, it is useful for calibrating mass flow controllers. Our experience with four-parameter HCLJ potential models for CF_4 and for C_2F_6 [5] provides confidence that the present HCLJ model for SF_6 can be extrapolated to 1000 K.

The Burnett $\rho(P, T)$ data extend to densities that are five times larger than the densities of the $u(P, T)$ data; thus, they could not be correlated using only two virial coefficients and the HCLJ model potential. In our preliminary correlation of these data, we excluded the $\rho(P, T)$ data on the near-critical isochore ($4380\ \mathrm{mol \cdot m^{-3}}$) and fitted the remaining $\rho(P, T)$ data and the $u(P, T)$ data simultaneously using a four-term virial equation of state. For this correlation, 13 parameters were used. Six parameters determined the temperature dependences of $B(T)$ and $C(T)$. These parameters appear in the algebraic expressions that relate $B(T)$ and $C(T)$ to separate hard-core square-well (HCSW) model intermolecular potentials. These algebraic expressions did not require the numerical integrations necessary with the HCLJ model. The two higher virial coefficients, $D(T)$

and $E(T)$, were represented by polynomial functions of $1/T$; four parameters were used for $D(T)$ and three were used for $E(T)$. It is unwise to extrapolate these polynomials outside of the range of the $\rho(P, T)$ data, $283\ \mathrm{K} \leqslant T \leqslant 393\ \mathrm{K}$. The 13-parameter $\{\mathrm{HCSW} + \mathrm{polynomials}\}$ model predicts accurate vapor densities closer to the coexistence curve and critical point than does the HCLJ model; however, it cannot be extrapolated safely. The HCSW model represents all of the present data except the $\rho(P, T)$ data on the critical isochore; thus, it demonstrates the internal consistency of these data and it was used to compare the present data with data from other laboratories.

2. EXPERIMENTAL

The equipment and techniques used to measure the speed of sound are described first; then, the Burnett apparatus is described. These apparatuses have been described elsewhere; thus, only an overview and references are provided.

2.1. Cylindrical Acoustical Resonator

Gillis et al. [6] and Gillis [7] described the cylindrical resonator, the model used to determine the speed of sound from the resonance data, and the resonator's performance. This apparatus has been used to study more than 20 gases and gas mixtures. Extensive results for seven gaseous halogenated hydrocarbons appear in Gillis [8]; extensive results for helium–xenon mixtures are given in Ref. 9.

The resonator was a heavy-walled stainless-steel cylindrical cavity 14 cm long with a 6.5-cm I.D. and a 7.8-cm O.D. Circular stainless-steel plates (1.3 cm thick) were bolted to the ends of the cavity and sealed to it with gold O-rings. Sound was generated and detected outside the resonator. Acoustic wave guides conducted sound from the generator (a commercially manufactured earphone speaker) to the resonator and then from the resonator to the detector (a commercially manufactured hearing aid). The sound entered and left the resonator through two thin diaphragms that were mounted flush with the interior surface of the cavity. These diaphragms were stainless-steel disks (1 cm in diameter, 25 μm thick) that separated the sample gas (SF_6) from argon that filled the waveguides.

When SF_6 was present in the resonator's cavity, a pressure controller maintained an equal pressure of argon in the wave guides and the transducer housings to insure that the thin metal diaphragms were not stretched by a differential pressure. The waveguides strongly attenuated sound at

frequencies above 8 kHz. Thus, the acoustic resonance frequencies above 8 kHz in the SF_6 were not measured.

Typically, the sound generator was scanned through two longitudinal, (3, 0, 0) and (4, 0, 0), modes and one radial, (0, 0, 1), mode. (The modes are labeled with the notation (K, N, S) used by Gillis [7].) The resonance frequencies f_{KNS} and half-widths g_{KNS} of these modes were measured using standard procedures and instruments [7]. Typically, the standard deviation of f_{KNS} was less than $10^{-5} f_{KNS}$. The values of f_{KNS} were corrected for the thermal and viscous losses at the boundaries and for the small effects of the tube used to admit SF_6 into and to remove it from the cavity [7]. The tabulated speed-of-sound data and their relative standard uncertainties (unless otherwise noted, coverage factor σ or $k = 2$) were computed from weighted averages of the results for the three modes. The relative standard uncertainties ranged from 10^{-5} to 10^{-4}, with the largest uncertainties occurring at the pressure extremes. At the highest pressures, the dominant contribution to the uncertainty resulted from inconsistent values of the speed of sound, as determined from the three modes. The inconsistencies increased approximately in proportion to the pressure P and had complicated temperature dependences. Most probably, they resulted from the interactions between the acoustic modes in the gas and the elastic response of the stainless-steel resonator. At the lowest pressures, the uncertainties increased because the signal-to-noise ratio decreased approximately as P^2.

The resonator was suspended in a well-stirred thermostated bath of either silicon oil or methanol, depending upon the temperature. The bath was controlled within 2 mK of each set-point. The temperature of the resonator was determined with a 25-Ω capsule-type standard platinum resistance thermometer (SPRT) that had been calibrated on ITS-90 and was embedded in an aluminum block fastened to the resonator. Four-wire resistance measurements of the SPRT were made with a suitable DC multimeter.

A 13-kPa full-scale differential pressure transducer (DPT) was used to measure the differential pressure between the argon and the SF_6. The DPT was calibrated for pressure and temperature dependences and was thermostated with a stability of ± 0.1 K. Pressure measurements were made on the argon side of the DPT with a quartz Bourdon-tube differential pressure gauge. The reference side of the gauge was maintained below 2 Pa with a rotary pump. This Bourdon-tube gauge had been calibrated with a deadweight gauge to a standard relative standard uncertainty of $\sigma_P = 30$ Pa $+ 0.0001P$.

Measurements were made along isotherms by initially loading the resonator to the lesser of 1.5 MPa or 80% of the vapor pressure of the SF_6. The temperature and pressure were allowed to equilibrate, and the frequencies

and widths of the acoustic resonances were measured. The pressure was reduced in successive steps. For each step, the air-operated valves were opened briefly and a portion of the SF_6 was collected in a vessel cooled with liquid nitrogen. After the pressure was reduced, the resonator was allowed to return to the equilibrium temperature and then the frequencies, half-widths, temperature, and pressure were measured in the new state.

The temperature-dependent effective radius $a(T)$ and length $l(T)$ of the cylindrical resonator were required to determine the speed of sound from the resonance frequencies. The functions $a(T)$ and $l(T)$ were determined by measuring the resonance frequencies when the resonator was filled with argon, a gas for which the speed of sound is accurately known. Because the calibration and the final measurements were conducted in the same bath, there is a high degree of compensation for the effects of temperature gradients in the bath and even for systematic uncertainties in the measurement of temperature.

2.2. Burnett Apparatus

Weber [10] described the Burnett apparatus in detail. The apparatus consisted of two cylindrical volumes: $V_1 \approx 27\ \text{cm}^3$ and $V_2 \approx 18\ \text{cm}^3$. These volumes had been bored out from opposite ends of a single nickel cylinder. The volume V_1 was called the "sample volume," and it was bound at one end by a highly sensitive, home-made, capacitance diaphragm differential pressure transducer (DPT). Helium expansions from the sample volume into the combined volumes were used to determine the cell constant $N \equiv (V_1 + V_2)/V_1 = = 1.781327 \pm 0.000035$. The thermal expansion of the volume V_1 between the temperature T and 273 K was accounted for by adjusting the densities using the equation

$$\rho_i = \left(\frac{\rho_0}{N^i}\right)\left(1 - \int_{T_0}^{T} \beta(T)\, dT\right) \tag{1}$$

which relates the density on the ith isochore to the volumetric thermal expansion coefficient $\beta(T)$. In Eq. (1), $T_0 \equiv 373$ K was the isotherm that was used for the Burnett expansions and ρ_0 was the initial density of the sample at 373 K. (ρ_0 is sometimes called the "run constant.") We used the function $\beta(T) = [37 + 0.038(T - 273)] \times 10^{-6}$, where $\beta(T)$ is in K^{-1} and T is in K, which was obtained from Ref. 11.

The DPT was used as a null detector when balancing the pressure of the SF_6 in the sample volume with the pressure of argon that filled the manifold that led from the DPT to the pressure gages and to a piston-type pressure controller. The argon pressure was measured with either a quartz

Bourdon-tube gauge or a pneumatic deadweight piston gauge in conjunction with a calibrated barometer. The sample volume and the expansion volume together with the piping and the DPT were located in a bath that was thermostated to within approximately 1 mK. The temperature was measured with a standard platinum resistance thermometer connected to a high-precision multimeter.

Automated pressure and temperature measurements were made on quasi-isochores and the densities of the quasi-isochores were determined by Burnett expansions on the single isotherm $T_0 = 373$ K. First, the sample volume V_1 was filled with SF_6 and then it was valved off at the highest pressure P_0 on the isotherm T_0. The temperature was reduced in steps under computer control, while the pressure was monitored with the quartz Bourdon-tube gauge. Thus, the equation of state was measured on the first quasi-isochore without operator intervention. (If the thermal and pressure expansion of V_1 could have been ignored, then the data would have been exactly on an isochore.) The apparatus was returned to T_0, and a single Burnett expansion was made to the pressure P_1. Then, the equation of state was measured on the second quasi-isochore starting at the state (P_1, T_0) and the apparatus was returned to T_0. This process was repeated until the Burnett expansions on T_0 brought the pressure to below 200 kPa. Through this procedure, the entire equation of state was measured with only slightly more effort than that required for a single Burnett isotherm. However, the accuracy was reduced for several reasons. One is that the quartz Bourdon-tube gauge was neither as accurate nor as stable as the piston gauge. When the pressure was measured manually with the Bourdon-tube gauge, its standard deviation was $\sigma_p = \sqrt{(50 \times 10^{-6} P)^2 + (37 \text{ Pa})^2}$. In automatic operation, the dead band of the pressure servosystem contributed an additional ± 80 Pa to the uncertainties of the pressure measurement. In that case, $\sigma_p = \sqrt{(50 \times 10^{-6} P)^2 + (88 \text{ Pa})^2}$.

2.3. Sample and Data

The SF_6 sample was obtained from a commercial vendor and identified as "VLSI (very large-scale integration) grade," with a certified purity of 99.995 %, by volume. Our own tests, made with a gas chromatograph, are consistent with the manufacturer's claim and they indicated that a single, volatile impurity (probably air) was present.

All of the Burnett measurements were made using a single sample of SF_6. This sample was degassed by three cycles of freezing, pumping, and thawing.

For the speed-of-sound measurements, a fresh sample of SF_6 was withdrawn from the supplier's container. Each sample was used to acquire the data on only one isotherm and then it was discarded. Each of these samples was degassed by several cycles of freezing, pumping, and thawing. We consider air as a typical impurity. If the SF_6 were contaminated by air in the concentration x (by mole fraction), the speed of sound would be increased by the factor $(1 + 0.4x)$. This factor is negligible because x was less than 5×10^{-5}, even before degassing.

Figure 1 displays temperature–pressure states spanned by the present measurements. They cover much of the region of interest to industry.

3. RESULTS

3.1. Speed-of-sound data $u(P, T)$

The speed-of-sound data are presented in Table I at 280 individual state points. Table I also lists the relative standard uncertainties of these measurements. The uncertainties are computed from the weighted average of the three values of the speed of sound obtained from the three acoustic modes.

3.2. Burnett Data $\rho(P, T)$

The Burnett vapor densities ρ at each of the 83 state points are presented in Table II. Because the analysis of the Burnett isotherm is nonlinear, the uncertainty of the gas densities is a complicated function of the uncertainty of the pressure measurements. We estimate that the relative standard uncertainty of the density is less than 0.02% for states with pressures above 2 MPa.

3.3. Vapor Pressure Data

During the Burnett experiments, two-phase states were encountered. In these cases, we recorded the vapor pressure measurements, although it was not our intention that these be definitive. Previous comparisons of vapor-pressure data collected with this apparatus to high-quality data collected in other laboratories show differences of the order of $\pm 0.2\%$ of the pressure [10, 12]. The present data are listed in Table III. Figure 2 compares our vapor pressure data with other measurements using the recent correlation by Totskii et al. [13] as a base line. Figure 2 shows that our vapor pressure data are among the lowest reported for SF_6; however, they are all within 0.35% of the data of Totskii et al. Weber [14] showed

Table I. Measured Speed of Sound in Sulfur Hexafluoride

P (kPa)	u ($m \cdot s^{-1}$)	$10^6\sigma[u]/u$
$T = 460.00$ K		
1500.6	162.967	66
1500.2	162.968	67
1500.0	162.969	68
1499.5	162.970	68
1499.2	162.971	66
1498.9	162.973	61
1419.7	163.200	69
1299.9	163.547	65
1232.4	163.745	57
1119.2	164.076	61
1018.5	164.376	53
900.69	164.726	47
822.77	164.963	41
714.52	165.288	36
608.02	165.613	35
512.76	165.905	25
412.44	166.216	26
$T = 440.00$ K		
1504.8	158.469	109
1429.2	158.737	109
1310.3	159.158	109
1201.1	159.546	92
1101.8	159.904	82
1003.3	160.255	80
913.78	160.578	81
807.50	160.960	59
714.74	161.297	52
614.53	161.662	23
503.74	162.072	16
411.76	162.411	22
358.24	162.610	13
307.30	162.800	27
254.06	162.997	41
205.50	163.181	47
$T = 420.00$ K		
1493.4	153.788	129
1422.0	154.096	129
1309.0	154.578	132
1218.8	154.969	112
1110.7	155.434	102
1025.5	155.803	103
948.75	156.135	89
811.27	156.735	69
712.36	157.167	34
602.64	157.646	34
511.43	158.047	25
407.64	158.502	13
358.48	158.720	7
302.91	158.965	26
256.04	159.170	24
205.83	159.392	35
151.16	159.633	52
101.24	159.854	84
$T = 400.00$ K		
1502.5	148.730	149
1434.9	149.082	144
1315.6	149.706	135
1217.0	150.222	124
1116.4	150.750	113
1023.2	151.237	103
908.63	151.836	86
808.83	152.357	59
719.34	152.826	51
604.16	153.428	48
509.05	153.927	29
402.39	154.485	28
360.00	154.706	29
305.33	154.993	27
252.31	155.270	29
205.96	155.513	36
151.91	155.797	43
100.95	156.061	81
1503.8	148.730	94
1435.3	149.088	93
1317.3	149.705	76
1219.7	150.217	65
1119.8	150.739	64
1028.0	151.218	61
918.30	151.789	65
820.58	152.301	61
711.41	152.871	62
603.67	153.434	53
514.33	153.901	48
404.68	154.473	31
357.64	154.719	30
293.63	155.053	34
234.96	155.363	63
$T = 380.00$ K		
1505.2	143.323	129
1441.9	143.728	135
1328.6	144.453	128
1225.1	145.114	121
1129.9	145.719	123
1012.6	146.462	111
907.62	147.126	92
813.29	147.721	92
705.58	148.401	73
614.36	148.971	63
508.13	149.637	51
406.20	150.273	39
353.10	150.605	34
308.59	150.881	31
256.88	151.202	26
204.66	151.527	36
153.64	151.842	39
101.92	152.164	140
$T = 360.00$ K		
1500.0	137.494	136
1440.8	137.966	130
1336.9	138.789	128
1236.3	139.581	125
1111.5	140.556	115
1026.3	141.216	96
920.61	142.029	91
802.56	142.931	81
719.82	143.562	72
607.54	144.410	65
514.19	145.112	53
406.08	145.920	38
359.98	146.261	39
302.28	146.690	31
258.12	147.017	26

Table I. *(Continued)*

P (kPa)	u ($m \cdot s^{-1}$)	$10^6\sigma[u]/u$
202.11	147.431	37
154.14	147.783	59
101.81	148.164	83
$T = 340.00$ K		
1498.3	130.999	128
1409.1	131.898	125
1323.4	132.752	124
1235.3	133.620	116
1119.6	134.746	104
1014.7	135.752	82
918.16	136.667	86
808.34	137.696	79
711.53	138.594	67
609.19	139.533	63
506.63	140.464	54
405.57	141.373	43
353.06	141.842	37
307.08	142.251	33
257.94	142.684	26
104.75	139.779	69
103.11	144.048	35
$T = 320.00$ K		
1499.8	123.523	145
1453.0	124.142	136
1408.4	124.726	137
1364.8	125.293	138
1322.5	125.836	133
1281.1	126.365	119
1217.4	127.166	111
1179.1	127.646	112
1120.1	128.372	97
1064.5	129.051	94
1030.3	129.466	93
977.99	130.090	84
914.56	130.843	80
863.81	131.440	85
814.84	132.008	81
772.61	132.496	76
714.23	133.162	60
670.33	133.661	68
636.05	134.048	62
565.55	134.836	58
506.70	135.487	46
467.86	135.911	47
427.98	136.346	39
392.18	136.734	33
353.08	137.156	28
315.15	137.562	22
274.78	137.992	22
234.54	138.417	21
193.60	138.850	36
153.42	139.272	58
148.04	139.326	45
137.03	139.442	54
127.14	139.546	55
116.55	139.655	56
104.75	139.779	69
94.43	139.886	60
84.03	139.996	79
73.23	140.106	83
$T = 300.00$ K		
1388.5	116.543	132
1327.2	117.622	130
1268.4	118.634	127
1233.4	119.226	121
1176.8	120.165	124
1122.5	121.051	122
1070.7	121.882	121
1020.5	122.675	116
972.09	123.426	112
925.55	124.137	100
865.60	125.039	89
822.96	125.675	84
768.62	126.471	83
718.27	127.199	72
682.80	127.705	64
633.59	128.401	59
579.14	129.160	56
521.90	129.947	56
471.25	130.634	43
417.11	131.358	42
363.60	132.066	29
310.49	132.760	21
255.32	133.473	16
231.16	133.783	26
215.75	133.980	32
201.55	134.160	19
188.34	134.328	33
173.72	134.513	34
160.46	134.681	42
145.80	134.863	37
131.68	135.043	52
116.93	135.226	55
102.95	135.402	60
$T = 280.00$ K		
1004.42	114.852	98
947.54	116.048	98
907.01	116.881	97
867.77	117.672	95
816.35	118.687	96
767.97	119.621	90
722.48	120.481	87
664.43	121.555	78
611.04	122.520	73
561.53	123.397	68
509.09	124.307	57
455.92	125.215	49
416.61	125.874	38
372.40	126.604	31
328.87	127.312	26
283.71	128.037	14
242.14	128.695	15
198.56	129.375	24
152.71	130.082	44
143.73	130.218	44
130.06	130.427	39
117.72	130.613	37
102.70	130.841	56
89.90	131.035	56
77.16	131.231	64
63.80	131.433	57
50.05	131.636	33

Table I. *(Continued)*

P (kPa)	u ($m \cdot s^{-1}$)	$10^6\sigma[u]/u$	P (kPa)	u ($m \cdot s^{-1}$)	$10^6\sigma[u]/u$	P (kPa)	u ($m \cdot s^{-1}$)	$10^6\sigma[u]/u$
$T = 270.00$ K			$T = 260.00$ K			354.99	118.037	31
802.43	114.973	76	613.82	115.366	56	310.25	119.087	38
765.89	115.798	78	566.29	116.495	44	255.00	120.342	58
717.47	116.866	80	515.06	117.674	45	213.77	121.257	53
666.51	117.959	84	463.61	118.824	53	174.74	122.098	39
618.24	118.971	52	409.59	119.994	50	$T = 240.00$ K		
562.52	120.105	49	359.47	121.051	41	401.20[a]	113.431	28
511.13	121.125	38	314.68	121.973	34	362.04[a]	114.534	23
462.06	122.076	21	274.93	122.773	39	308.61	115.981	11
411.11	123.043	26	231.89	123.625	41	256.53	117.340	8
356.20	124.061	28	187.41	124.487	71	202.42	118.699	49
307.55	124.944	19	143.93	125.313	44	154.40	119.866	61
284.60	125.356	30	102.73	126.086	43	102.91	121.072	90
256.90	125.845	18	$T = 250.00$ K			$T = 230.00$ K		
231.48	126.292	40	551.97[a]	113.027	51	221.41	115.225	40
199.54	126.848	40	516.11[a]	113.993	48	194.68	115.980	42
165.46	127.432	45	457.93	115.508	43	162.61	116.867	10
133.77	127.962	64	410.17	116.701	37	131.43	117.714	58
101.54	128.515	98						

[a] Pressure is greater than 80% saturated vapor pressure, sound speed is possibly affected by precondensation effects.

how static vapor pressure measurements are affected by sample purity. It is unlikely that the differences between our data and the previously published sets of data can be explained by the impurities known to be in our sample of SF_6.

4. ANALYSIS

4.1. Ideal-Gas Heat Capacities $C_P^0(T)$

The first step in analyzing the speed-of-sound data was to fit the data on each isotherm by the acoustical virial equation,

$$u^2 = \frac{\gamma^0 RT}{M}\left(1 + \frac{\beta_a P}{RT} + \frac{\gamma_a P^2}{RT} + \frac{\delta_a P^3}{RT} + \cdots\right) \tag{2}$$

Here, M is the molar mass of SF_6, R is the universal gas constant, γ^0 is the ideal-gas heat-capacity ratio defined by $\gamma^0(T) \equiv C_P^0(T)/C_V^0(T)$, and $\beta_a(T)$,

Table II. Burnett $\rho(P, T)$ Measurements

T/K	P/MPa	ρ/(kg·m^{-3})	T/K	P/MPa	ρ/(kg·m^{-3})	T/K	P/MPa	ρ/(kg·m^{-3})
371.60	7.48079	4377.50	363.15	3.28625	1380.11	371.15	1.24950	434.83
371.60	7.48144	4377.50	371.11	3.40690	1379.68	371.68	1.25167	434.82
373.15	7.58875	4377.23	371.68	3.41518	1379.65	371.68	0.72520	244.11
383.13	8.28095	4375.52	371.68	2.10995	774.54	373.17	0.72754	244.10
393.14	8.97130	4373.81	373.17	2.12146	774.49	393.17	0.77096	243.90
333.15	4.78808	4384.09	383.20	2.19679	774.19	283.18	0.53338	244.96
343.17	5.49451	4382.37	393.18	2.27163	773.88	293.14	0.55543	244.86
353.15	6.19374	4380.66	283.20	1.40787	777.22	303.18	0.57752	244.76
363.17	6.89253	4378.94	293.12	1.49150	776.92	313.18	0.59935	244.67
371.59	7.48041	4377.50	303.12	1.57399	776.61	323.20	0.62110	244.57
371.67	5.19270	2457.52	313.13	1.65496	776.31	333.18	0.64276	244.48
373.17	5.23916	2457.37	323.11	1.73455	776.01	343.18	0.66426	244.38
383.21	5.55350	2456.41	333.15	1.81357	775.70	353.17	0.68564	244.29
393.16	5.86186	2455.45	343.12	1.89125	775.40	363.16	0.70642	244.19
338.10	4.11042	2460.75	353.13	1.96847	775.10	371.16	0.72402	244.11
348.14	4.44031	2459.78	363.14	2.04508	774.79	371.68	0.72513	244.11
358.16	4.76385	2458.82	371.09	2.10554	774.55	371.68	0.41435	137.04
368.16	5.08203	2457.86	371.67	2.10997	774.54	283.19	0.30992	137.52
371.70	5.19399	2457.52	371.65	1.25146	434.82	293.14	0.32178	137.46
371.68	3.41520	1379.65	373.17	1.25782	434.80	303.12	0.33369	137.41
373.17	3.43749	1379.57	383.16	1.29687	434.63	313.14	0.34564	137.36
383.18	3.58770	1379.03	393.17	1.33624	434.46	323.20	0.35756	137.30
393.17	3.73626	1378.49	313.16	1.01619	435.82	333.18	0.36933	137.25
313.13	2.49688	1382.81	323.15	1.05703	435.65	343.17	0.38089	137.20
323.15	2.66094	1382.27	333.15	1.09770	435.48	353.17	0.39259	137.14
333.15	2.82084	1381.73	343.17	1.13808	435.31	363.16	0.40441	137.09
343.16	2.97842	1381.19	353.17	1.17807	435.14	371.16	0.41360	137.05
353.13	3.13297	1380.65	363.15	1.21781	434.97			

Table III. Vapor Pressure Measured with the Burnett Apparatus

T (K)	P (MPa)	T (K)	P (MPa)
278.132	1.43447	293.187	2.10099
283.159	1.63611	298.127	2.36164
283.192	1.63622	303.132	2.65435
288.195	1.85798	308.144	2.97180
293.155	2.09699	313.141	3.32150

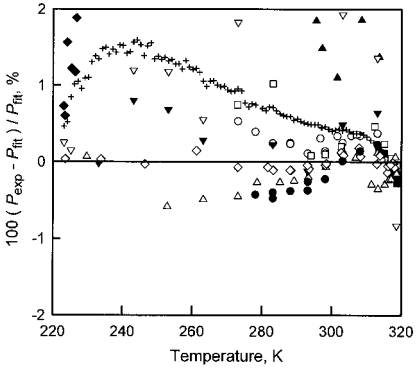

Fig. 2. Deviations (percentage) of vapor pressure data from the correlation of Totskii et al. [13]. (●) Present results; (◇) Totskii et al. [13]; (■) Biswas et al. [31, 53]; (○) Watanabe and Watanabe [32]; (✚) Borisoglebskii et al. [35]; (▲) Elma [36]; (▼) Ulybin and Zherdev [37]; (△) Mears et al. [44]; (□) Clegg and Rowlinson [43]; (▽) Miller et al. [38]; (◆) Schumb and Gamble [39].

$\gamma_a(T)$, and $\delta_a(T)$, are temperature-dependent acoustic virial coefficients. The fit of Eq. (2) to each isotherm yielded the acoustic virial coefficients and γ^0 at each temperature. The values of γ^0 were used to obtain $C_P^0(T)$ from the relation $C_P^0(T)/R = \gamma^0/(\gamma^0 - 1)$ and the results are listed in Table IV. At the two lowest temperatures, the values of $C_P^0(T)$ resulting from the fit of Eq. (2) are not reliable because the maximum pressure of the $u(P, T)$ data was restricted by the vapor pressure and because the contributions of the virial coefficients to the fit were large. Thus, the 230 K isotherm was not fitted by Eq. (2); the 240 K isotherm was fitted, however, the tabulated value of $C_P^0(T)$ has a large relative standard uncertainty of 1.2%. The other values of $C_P^0(T)/R$ in Table IV ($T \geqslant 250$ K) were fitted by polynomial functions of T to obtain

$$\frac{C_P^0(T)}{R} = -3.1283 + 7.335 \times 10^{-2}\left(\frac{T}{\mathrm{K}}\right) - 9.160 \times 10^{-5}\left(\frac{T}{\mathrm{K}}\right)^2 + 3.865 \times 10^{-8}\left(\frac{T}{\mathrm{K}}\right)^3 \qquad (3)$$

$$250\ \mathrm{K} \leqslant T \leqslant 460\ \mathrm{K}$$

Table IV. Ideal-Gas Heat Capacities $C_P^0(T)/R$ from Fitting Eq. (2) to the Data on Each Isotherm

T (K)	C_P^0/R	T (K)	C_P^0/R	T (K)	C_P^0/R
460	15.004	380	13.644	280	11.082
440	14.674	360	13.208	270	10.758
420	14.396	340	12.726	260	10.426
400	14.027	320	12.232	250	10.089
400	14.040	300	11.680	240	9.766[a]

[a] 1.2% relative standard uncertainty; see text.

The root-mean-square deviation of the residuals from the fit was 0.011, a value consistent with our previous experience with this apparatus and with the assertion that the relative standard uncertainty of the tabulated values of $C_P^0(T)/R$ is approximately 0.1% in the range $T \geqslant 250$ K. We believe that our values of $C_P^0(T)$ are the most accurate available in the temperature range $250\ \text{K} \leqslant T \leqslant 460\ \text{K}$.

Figure 3 (top) compares the values of $C_P^0(T)$ from Table IV to data from the literature. Figure 3 (bottom) shows the deviations of $C_P^0(T)/R$ from Eq. (3). Among the literature values of $C_P^0(T)$, those calculated for the JANAF Tables [15] are considered to be more accurate than the earlier calculations by Meyer and Buell [16], Gaunt [17], and Morsy [18]. The function given by Cole and de Reuck [4] spans a large temperature range and fits the JANAF values well. For these reasons, we recommend its use for temperatures outside of our experimental range. Beir et al. [19] claimed that their experimental results have an uncertainty of 1.0%; thus, they agree with our own, within the combined uncertainties. Eucken and Bertram [20] claimed experimental uncertainties between 0.5 and 1%, and Eucken and Ahrens [21] claimed uncertainties of 1.0 to 2.0%. Their data are in reasonable agreement with our own.

4.2. Virial Equation of State

Further analyses of our results are based on the density virial equation of state:

$$P = RT\rho[1 + B(T)\,\rho + C(T)\,\rho^2 + D(T)\,\rho^3 + \cdots] \tag{4}$$

In Eq. (4), the coefficients $B(T)$, $C(T)$, $D(T)$, etc., are the second, third, and fourth virial coefficients, respectively. We truncated the series at different terms, depending upon the range of the data to be correlated.

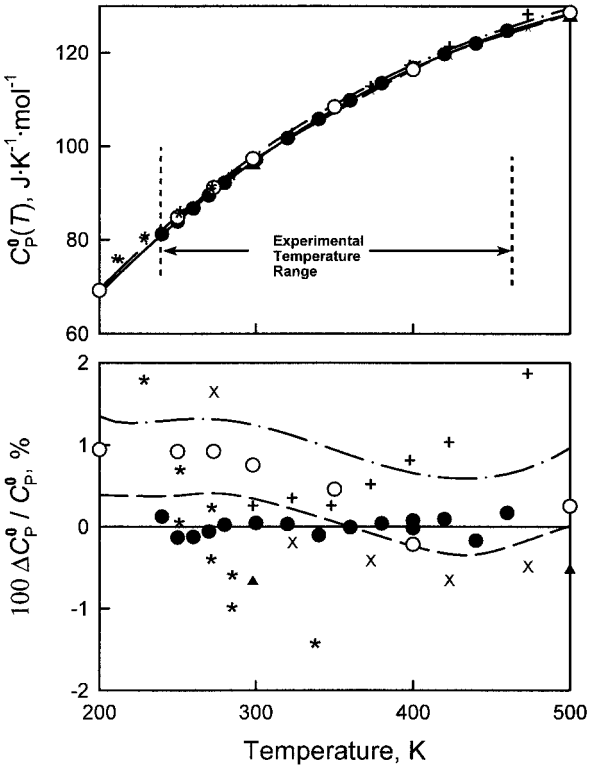

Fig. 3. Top: Ideal-gas heat capacities $C_P^0(T)$. Bottom: Fractional deviations of $C_P^0(T)$ from Eq. (3), where $\Delta C_P^0 = (C_{P,\,obs}^0 - C_{P,\,Eq.\,(3)}^0)$. (●) Present work; (——) Eq. (3); (– – –) Chase et al. [15]; (✚) Beir et al. [19]; (—— •) Morsy [18]; (○) Gaunt [17]; (▲) Meyer and Buell [16]; (×) Eucken and Bertram [20]; (∗) Eucken and Ahrens [21].

4.2.1. Hard-Core Lennard–Jones (HCLJ) Potential Model

The speed-of-sound measurements, except for a few measurements near the vapor–liquid coexistence curve, were correlated using Eq. (4) with the virial series truncated after $B(T)$ and $C(T)$. Following Trusler [22], we used a model intermolecular potential energy function to represent the temperature dependences of $B(T)$ and $C(T)$. Trusler [22] used the intermolecular potential of Maitland and Smith [23] to correlate speed-of-sound data for propane. We obtained better results using the hard-core Lennard–Jones (HCLJ) intermolecular potential function [24]:

$$\varphi(r_{ij}) = \varepsilon \frac{n}{n-m}\left(\frac{n}{m}\right)^{m/(n-m)} \left\{\left(\frac{\sigma-2a}{r_{ij}-2a}\right)^n - \left(\frac{\sigma-2a}{r_{ij}-2a}\right)^m\right\} \tag{5}$$

Here ε is the well depth, σ is the value of r where $\varphi(r)$ crosses zero, a is the radius of the hard core, r_{ij} is the distance between molecule i and molecule j, and, in the case of the 6–12 potential, $n=12$ and $m=6$. Given values, ε and a, we calculated the classical second and third virial coefficients and their temperature derivatives following Mason and Spurling [25] and Dulla et al. [26]. The calculation of the third virial coefficient requires the inclusion of three-body contributions. Following Trusler, we used the Axilrod–Teller triple–dipole term [27]:

$$\varphi(r_{123}) = \frac{\nu_{123}(1+\cos\theta_1\cos\theta_2\cos\theta_3)}{(r_{12}^3 r_{13}^3 r_{23}^3)^{-1}} \tag{6}$$

where ν_{123} is the dispersion coefficient and θ_i is defined as the angle subtended at molecule i by molecules j and k. This is the first term in the three-body corrections to the dispersion energy for monoatomic species. The integral equations providing the second and third virial coefficients for spherically symmetric molecules are given by

$$B(T) = -2\pi N_{\mathrm{A}} \int_0^\infty f_{12} r_{12}^2 dr_{12} \tag{7}$$

$$C(T) = -\frac{8\pi^2 N_{\mathrm{A}}^2}{3} \int_0^\infty \int_0^\infty \int_{|r_{12}-r_{13}|}^{|r_{12}+r_{13}|} (f_{12}f_{13}f_{23} - e_{12}e_{13}e_{23}f_{123}) \times r_{12} r_{13} r_{23}\, dr_{12}\, dr_{13}\, dr_{23} \tag{8}$$

where N_{A} is Avogadro's number and r_{ij} is the distance between molecule i and molecule j, $e_{ij} = \exp\{-\varphi(r_{ij})/k_{\mathrm{B}}T\}$, $f_{ij} = e_{ij} - 1$, and $f_{ijk} = \exp\{-\varphi(r_{ijk})/k_{\mathrm{B}}T\} - 1$. Equations (7) and (8) are used to calculate the density virial coefficients, $B(T)$ and $C(T)$, for a given intermolecular potential. However, the correlation of speed-of-sound data as a function of pressure on isotherms $u(P, T)$ requires the acoustic virial coefficients that appear in the acoustic virial equation of state, Eq. (2). In the fitting routine, we calculated the acoustic virial coefficients from the density virial coefficients, their temperature derivatives, $\gamma^0(T) = C_{\mathrm{P}}^0(T)/C_{\mathrm{V}}^0(T)$, and the expression for $C_{\mathrm{P}}^0(T)$ given in Eq. (3) using the thermodynamic relations provided by Gillis and Moldover [28].

For fitting the HCLJ potential, there were only four parameters, ε, σ, a, and ν_{123} to be adjusted using a nonlinear fitting routine. Initial guesses of ε, σ, and a were obtained by a preliminary fit to the second virial coefficient values obtained from the literature. The initial guess of ν_{123} was $\nu_{123} = 3\alpha C_6/4 = 0.0139\ \mathrm{K \cdot nm^9}$, where $\alpha = 4.549 \times 10^{-3}\ \mathrm{nm^3}$ is the mean polarizability of the SF_6 molecule [2] and $C_6 = 4.06201\ \mathrm{K \cdot nm^6}$ is the leading isotropic

Table V. Parameters for the HCLJ Potential

Parameter	Value
σ	0.4781 nm
ε	442.552 K
a	0.091396 nm
ν_{123}/k_B	0.02600 K · nm^9

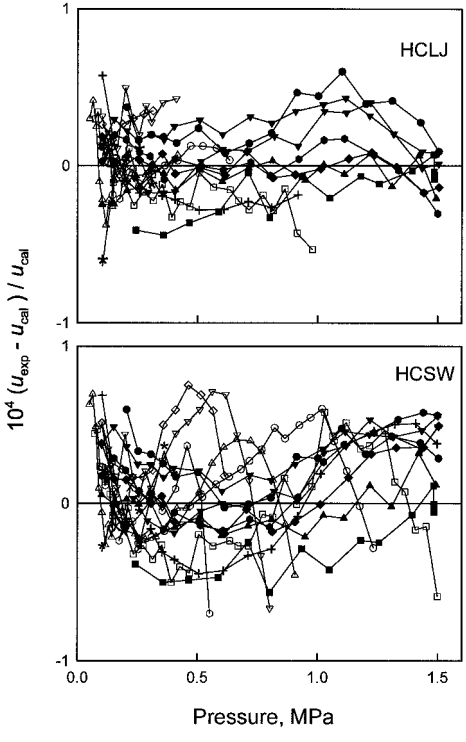

Fig. 4. Fractional deviations of the speed-of-sound data $[(u_{obs.} - u_{cal})/u_{cal}]$ from calculations using the fitted virial equations of state. Top: The baseline is the HCLJ model fitted solely to the $u(P, T)$ data. Bottom: The baseline is HCSW model deduced from the simultaneous fit to the $u(P, T)$ data and the Burnett measurements. (■) 460 K; (●) 440 K; (▲) 420 K; (▼) 400 K; (◆) 380 K; (⬢) 360 K; (✚) 340 K; (□) 320 K; (○) 300 K; (△) 280 K; (▽) 270 K; (◇) 260 K; (⬡) 250 K; (∗) 240 K; (✖) 230 K.

two-molecule dispersion coefficient calculated by Kumar et al. [29]. All four parameters were then varied to obtain the results in Table V. Figure 4 (top) shows the deviations of the speed-of-sound data from that calculated using the virial equation of state truncated after $B(T)$ and $C(T)$ as computed from the HCLJ potential using the parameters listed in Table V. Nearly all the data are within 0.005% of the fit. The final fit used 220

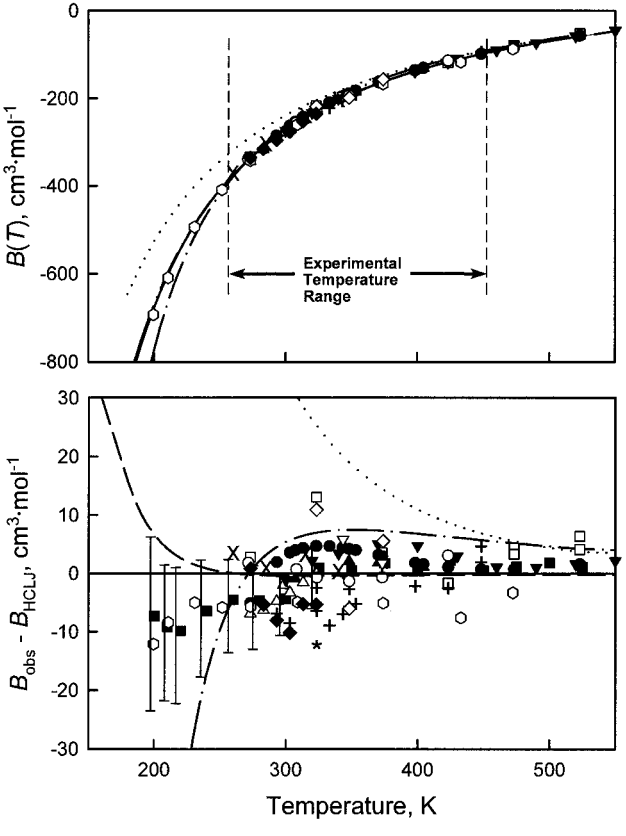

Fig. 5. Top: The second virial coefficient $B(T)$ as a function of the temperature. Bottom: Deviations of $B(T)$ from the HCLJ potential model. (——) HCLJ; (– – –) HCSW; (·····) Meinander potential [2]; (·–·–) Aziz et al. potential [1]; (■) Dymond and Smith [40]; (□) MacCormack and Schneider [41]; (✚) Hamann et al. [42]; (▲) Clegg and Rowlinson [43]; (△) Dymond and Smith [40]; (●) Mears et al. [44]; (▽) Hajjar and MacWood [45]; (∗) Nelson and Cole [46]; (▼) Bellm et al. [47]; (○) Sigmund et al. [48]; (★) Hahn et al. [49]; (◇) Hosticka and Bose [50]; (◆) Santafe et al. [51]; (✖) Mollerup [52].

speed-of-sound state points that remained after eliminating those near the vapor pressure curve which required higher virial coefficients. The fit had $v = 216$ degrees of freedom, and χ^2/v was 0.30.

Figure 5 (top) shows the second virial coefficient $B(T)$ determined from the present HCLJ model and the differences between this model and previously published results (bottom). The HCLJ values of $B(T)$ agree with most of the published data within their uncertainty and they extrapolate extremely well at temperatures both above and below our experimental range.

Figure 5 also shows values of $B(T)$ calculated from two previously published, isotropic model intermolecular potentials. One potential is a five-parameter model that Aziz et al. [1] fitted to viscosity data, and the second is a six-parameter model that Meinander [2] fitted to viscosity data and to his own collision-induced light-scattering measurements. Meinander also considered second-virial-coefficient data; however, he placed more weight on his own data.

The results for the third virial coefficient $C(T)$ are shown in Fig. 6. There are few previously published values of $C(T)$ to compare with; the present HCLJ model passes right through them. We also calculated $C(T)$ using the potentials of Aziz and of Meinander assuming that $\nu_{123} = 0.0139\ \mathrm{K \cdot nm^9}$, the value that was used as an initial guess, as discussed above. At temperatures above our experimental temperature range, the

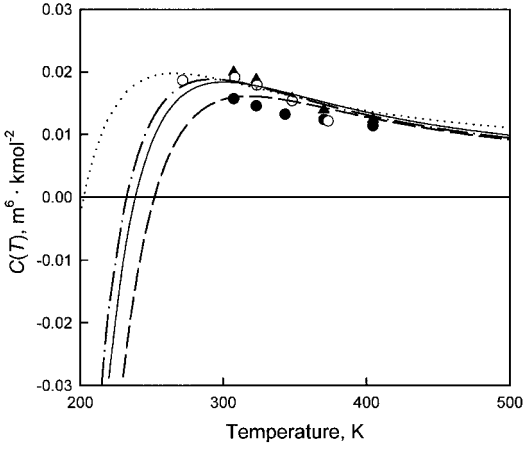

Fig. 6. The third virial coefficient as a function of the temperature. (——) HCLJ; (– – –) HCSW; (· · · · · ·) Meinander potential [2]; (· – · – ·) Aziz et al. potential [1]; (▲) Clegg and Rowlinson [43]; (●) Mears et al. [44]; (○) Sigmund et al. [48].

values of $C(T)$ calculated from the potential of Aziz et al. [1] are close to those calculated from the present HCLJ model. The values of $C(T)$ calculated from the potential of Meinander [2] are much larger than the HCLJ values, especially at the lower temperatures. At the same temperatures, his values of $B(T)$ also diverge from the HCLJ values.

In our opinion, the virial coefficients calculated from the present HCLJ potential will provide reasonable estimates of the density of gaseous SF_6 from its triple point to conditions where it begins to ionize.

The calculation of $B(T)$ and $C(T)$ from Eqs. (7) and (8) is complicated; thus, it is time-consuming when used for repetitive calculations and it is inconvenient to program. To mitigate these problems, we tabulated $B(T)$ and $C(T)$ and their first two temperature derivatives and, below, we recommend a method of interpolation. To prepare Table VI, we defined the reduced reciprocal temperature $\tau = \varepsilon/k_{\mathrm{B}}T$ with $\varepsilon = 442.552$ K. In this variable, Table VI spans the range $0.3 \leqslant \tau \leqslant 3.0$, corresponding to $147\ \mathrm{K} \leqslant T \leqslant 1470\ \mathrm{K}$. These ranges greatly exceed our experimental temperature ranges; however, the extrapolations are justified by their agreement with other published data in these regions. In Table VI the virial coefficients are presented in reduced (unitless) forms defined by $B^*(T) \equiv B(T)/b_0$, $C^*(T) \equiv C(T)/b_0^2$, and $b_0 \equiv 2\pi N_{\mathrm{A}}\sigma^3/3$. The derivatives of the virial coefficients with respect to T are related to the tabulated derivatives with respect to τ through

$$T\frac{dB}{dT} = -\tau\frac{dB}{d\tau} \qquad \text{and} \qquad T^2\frac{d^2B}{dT^2} = \tau^2\frac{d^2B}{d\tau^2} + 2\tau\frac{dB}{d\tau}$$

For evaluating $B^*(\tau)$, $C^*(\tau)$, and their derivatives, at the reduced temperature τ between adjacent points at τ_1 and τ_2, we recommend using the cubic polynomial $f(\tau)$ such that

$$\begin{aligned} f(\tau) &= a(\tau-\tau_1) + b(\tau-\tau_2) + \{c(\tau-\tau_1) + d(\tau-\tau_2)\}(\tau-\tau_1)(\tau-\tau_2) \\ a &= f(\tau_2)/\Delta\tau, \qquad c = \{f'(\tau_2)/(\Delta\tau)^2\} - \{(a+b)/(\Delta\tau)^2\} \\ b &= -f(\tau_1)/\Delta\tau, \qquad d = \{f'(\tau_1)/(\Delta\tau)^2\} - \{(a+b)/(\Delta\tau)^2\} \end{aligned} \tag{2}$$

where $f' = df/d\tau$ and $\Delta\tau = \tau_2 - \tau_1$. To allow the calculation of the second derivatives, the third derivatives are included in Table VI.

The results of the interpolation are very accurate. The differences between the interpolated and directly [using Eqs. (7) and (8)] calculated values of $B(T)$ and $T\,dB(T)/dT$ are less than 0.01 and 0.05 $\mathrm{cm^3 \cdot mol^{-1}}$, respectively. The differences between the interpolated and the directly calculated values of $C(T)$, $T\,dC(T)/dT$, and $T^2\,d^2C(T)/d^2T$ are 1.0, 2.5,

Table VI. SF_6 Reduced Virial Coefficients and Their Derivatives with Reduced Temperature

τ	$B^*(\tau)$	$\frac{\partial B^*(\tau)}{\partial \tau}$	$\frac{\partial^2 B^*(\tau)}{\partial \tau^2}$	$\frac{\partial^3 B^*(\tau)}{\partial \tau^3}$	$C^*(\tau)$	$\frac{\partial C^*(\tau)}{\partial \tau}$	$\frac{\partial^2 C^*(\tau)}{\partial \tau^2}$	$\frac{\partial^3 C^*(\tau)}{\partial \tau^3}$
0.3	0.48425	−1.30391	−1.61004	5.16410	0.3643	−0.1213	0.5414	8.5865
0.4	0.34647	−1.44662	−1.30059	1.68367	0.3561	−0.0333	1.1507	4.3215
0.5	0.19552	−1.57081	−1.20379	0.43206	0.3592	0.0999	1.4813	2.4780
0.6	0.03246	−1.69016	−1.19269	−0.14680	0.3769	0.2582	1.6659	1.2538
0.7	−0.14256	−1.81077	−1.22496	−0.47251	0.4112	0.4292	1.7335	0.0799
0.8	−0.32985	−1.93602	−1.28365	−0.68942	0.4628	0.6007	1.6744	−1.3178
0.9	−0.52999	−2.06812	−1.36121	−0.85623	0.5309	0.7588	1.4558	−3.1411
1.0	−0.74376	−2.20877	−1.45414	−1.00001	0.6135	0.8848	1.0253	−5.5922
1.1	−0.97208	−2.35941	−1.56091	−1.13466	0.7060	0.9543	0.3086	−8.9081
1.2	−1.21602	−2.52140	−1.68103	−1.26799	0.8013	0.9337	−0.7950	−13.3847
1.3	−1.47678	−2.69607	−1.81463	−1.40487	0.8883	0.7780	−2.4196	−19.4007
1.4	−1.75570	−2.88479	−1.96224	−1.54865	0.9504	0.4266	−4.7426	−27.4459
1.5	−2.05425	−3.08901	−2.12467	−1.70186	0.9644	−0.2015	−7.9973	−38.1549
1.6	−2.37407	−3.31025	−2.30299	−1.86662	0.8974	−1.2140	−12.4895	−52.3519
1.7	−2.71693	−3.55018	−2.49845	−2.04485	0.7041	−2.7539	−18.6193	−71.1070
1.8	−3.08478	−3.81056	−2.71247	−2.23841	0.3228	−5.0097	−26.9088	−95.8099
1.9	−3.47979	−4.09335	−2.94670	−2.44915	−0.3299	−8.2301	−38.0391	−128.2646
2.0	−3.90427	−4.40064	−3.20294	−2.67902	−1.3662	−12.7415	−52.8974	−170.8128
2.1	−4.36081	−4.73473	−3.48321	−2.93007	−2.9354	−18.9719	−72.6384	−226.4942
2.2	−4.85219	−5.09815	−3.78973	−3.20448	−5.2363	−27.4815	−98.7642	−299.2540
2.3	−5.38150	−5.49364	−4.12496	−3.50464	−8.5318	−39.0020	−133.2275	−394.2125
2.4	−5.95209	−5.92419	−4.49161	−3.83313	−13.1686	−54.4887	−178.5660	−518.0160
2.5	−6.56762	−6.39310	−4.89263	−4.19275	−19.6028	−75.1866	−238.0769	−679.2920
2.6	−7.23211	−6.90397	−5.33130	−4.58659	−28.4332	−102.7178	−316.0432	−889.2421
2.7	−7.94995	−7.46074	−5.81120	−5.01801	−40.4439	−139.1940	−418.0279	−1162.4121
2.8	−8.72593	−8.06772	−6.33627	−5.49070	−56.6608	−187.3625	−551.2565	−1517.6953
2.9	−9.56532	−8.72964	−6.91085	−6.00871	−78.4240	−250.7965	−725.1142	−1979.6382
3.0	−10.47386	−9.45169	−7.53967	−6.57648	−107.4823	−334.1420	−951.7922	−2580.1404

and 15.0 $cm^6 \cdot mol^{-2}$, respectively. The largest interpolation errors occur at the lowest temperatures for $C(T)$. Even there, the interpolation errors in calculating, for example, the vapor density are much smaller than the errors from the uncertainties of $C(T)$ itself.

4.2.2. Hard-Core Square-Well Potential Model

The virial equation of state presented in Section 4.2.1 with $B(T)$ and $C(T)$ determined by the hard-core Lennard–Jones potential model is satisfactory for the densities encountered in our speed-of-sound measurements. We now consider a virial equation of state that is valid at the higher densities (and pressures) reached by the Burnett $\rho(P, T)$ measurements. This requires the inclusion of the higher virial terms in Eq. (4), i.e., $D(T)$ and $E(T)$. At present, it is not practical to compute $D(T)$ and $E(T)$ from realistic model intermolecular potentials such as the HCLJ model. We adopted the expedient, frequently-used alternative of representing $D(T)$ and $E(T)$ as polynomial functions of the inverse temperature:

$$D(T) = \sum_{n=0}^{3} d_n T^{-n} \qquad \text{and} \qquad E(T) = \sum_{n=0}^{2} e_n T^{-n} \tag{3}$$

When introducing this empirical representation of $D(T)$ and $E(T)$, we also chose to simplify the representations of $B(T)$ and $C(T)$ in comparison with integral representations used in Eqs. (7) and (8). Thus, we used the algebraic expressions of the temperature provided by the hard-core square-well (HCSW) model intermolecular potential to represent $B(T)$ and $C(T)$. Hurly et al. [30] successfully used the HCSW expressions to fit speed-of-sound and Burnett measurements simultaneously for the helium–xenon mixtures. Because the temperature derivatives of the HCSW expressions for $B(T)$ and $C(T)$ can be calculated explicitly, it was straightforward to determine the acoustical virial coefficients from the density virial coefficients and $C_P^0(T)$ using the exact thermodynamic relations given in Gillis and Moldover [28]. In contrast with the frequently used inverse-T polynomial functions, the HCSW expressions extrapolate well to high temperatures, although not as well as the more realistic hard-core Lennard–Jones model.

The HCSW parameters are related to $B(T)$ and $C(T)$ by

$$\begin{aligned} B(T) &= b_0[1 - (\lambda^3 - 1)\,\Delta] \\ C(T) &= \tfrac{1}{8} b_0^2 (5 - c_1\Delta - c_2\Delta^2 - c_3\Delta^3) \end{aligned} \tag{4}$$

$$\begin{aligned} c_1 &= \lambda^6 - 18\lambda^4 + 32\lambda^3 - 15 \\ c_2 &= 2\lambda^6 - 36\lambda^4 + 32\lambda^3 + 18\lambda^2 - 16 \\ c_3 &= 6\lambda^6 - 18\lambda^4 + 18\lambda^2 - 6 \end{aligned} \tag{5}$$

where $\Delta = e^{\varepsilon/k_B T} - 1$ and k_B is Boltzmann's constant. The adjustable parameters are as follows: ε is the well depth, λ is the ratio of the width of the well to the diameter σ of the hard core, where the molar volume of the hard core $b_0 = \frac{2}{3}\pi N_A \sigma^3$, and N_A is Avogadro's number. We allowed each virial coefficient to have its own value for ε, λ, and σ; thus, we do not attribute physical significance to the values that resulted from fitting the data.

Thus, the HCSW model had 13 adjustable parameters, 3 each for $B(T)$, $C(T)$, and $E(T)$ and 4 for $D(T)$. We determined these parameters using a simultaneous fit to the measured $u(P, T)$ and $\rho(P, T)$ results. The fitting routine used Eqs. (3)–(5), their temperature derivatives, Eq. (3) for $C_P^0(T)$, and the thermodynamic relations from Ref. 28 to compute the acoustic virial coefficients. In turn, these were substituted into Eq. (2) to determine the density virial coefficients in Eq. (4). The best fit parameters are given in Table VII. The fit had $\nu = 279$ degrees of freedom and a reduced chi-square $\chi^2/\nu = 0.768$. The deviations of the $u(P, T)$ data from those calculated from the HCSW model are displayed in the lower panel in Fig. 4. Nearly all speed-of-sound data are reproduced to within 0.005%. The figure includes the $u(P, T)$ data at higher pressures near the vapor–liquid coexistence curve that were not included in the fit to the HCLJ model.

Figure 7 shows the differences between the pressures measured in the Burnett apparatus and those calculated from the 13-parameter HCLJ virial equation of state. The dashed lines at $\pm 0.015\%$ indicate that most of the data are consistent with the fit to this level. At pressures below 2 MPa, the relative uncertainty of the pressure measurements increases above 0.015% and this is evident in Fig. 7.

The values of $B(T)$ determined with the HCSW model are almost-indistinguishable from those determined of the HCLJ model, as shown in the upper panel in Fig. 5. The lower panel in Fig. 5 shows the differences between the data from several sources and the HCLJ model. The HCSW is significantly different from the HCLJ model only when the reduced temperature $T^* \equiv T/T_c < 0.8$, where $B(T)$ from the HCSW model is known to be incorrect [28].

The values of $C(T)$ obtained from the HCSW model are close to those obtained by us with the HCLJ model and those obtained by other authors except below $T^* < 1$. (See Fig. 6.) The present 13-parameter HCSW model can be used to calculate vapor densities up to 80% of the vapor pressure or 2500 mol · m^{-3} in the temperature range 230 K $\leqslant T \leqslant$ 460 K.

Figure 8 compares the present $\rho(P, T)$ data with previously published equation-of-state data on the isotherm at 333 K. The baseline for this comparison is the equation of state developed by Cole and de Reuck [4]. On

Table VII. Best Fit Parameters for Virial Equation of State Determined from a Simultaneous Fit to Speed-of-Sound and Burnett Measurements

	$B(T)$ $(m^3 \cdot mol^{-1})$	$C(T)$ $(m^6 \cdot mol^{-2})$		$D(T)$ $(m^9 \cdot mol^{-3})$		$E(T)$ $(m^{12} \cdot mol^{-4})$
$10^4 b_0$ $(m^3 \cdot mol^{-1})$	1.233137	1.377322	d_0	-1.55516×10^{-11}	e_0	-1.11930×10^{-16}
λ	1.447872	1.408264	d_1	2.04614×10^{-8}	e_1	3.03261×10^{-13}
ε/k_B (K)	283.5533	297.1584	d_2	-9.22781×10^{-6}	e_2	-1.03129×10^{-10}
			d_3	1.41098×10^{-3}		

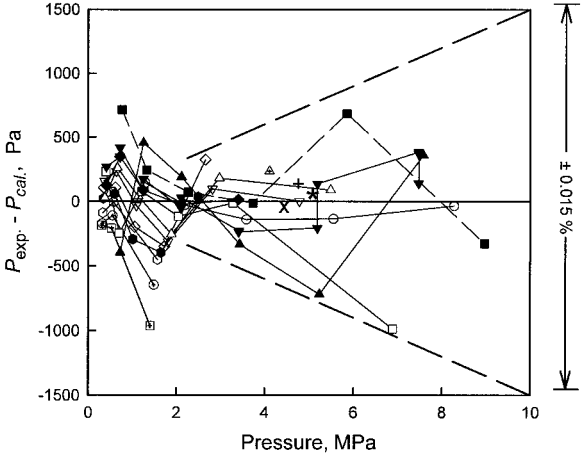

Fig. 7. Differences of the pressure measured with the Burnett apparatus from the prediction of the HCSW equation of state deduced from the simultaneous fit to the $u(P, T)$ data and the Burnett measurements. The dashed lines indicate deviations of $\pm 0.015\%$. (⊞) 283 K; (⊕) 293 K; (⬢) 303 K; (⬡) 313 K; (◇) 323 K; (▽) 333 K; (◬) 338 K; (△) 343 K; (✖) 348 K; (○) 353 K; (✚) 358 K; (□) 363 K; (∗) 368 K; (◆) 371 K; (▼) 372 K; (▲) 373 K; (●) 383 K; (■) 393 K.

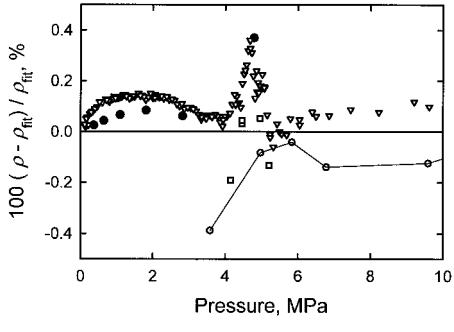

Fig. 8. Deviations of measured densities along the 333 K isotherm from that predicted from the Cole and de Reuck [4] equation of state. (●) Present Burnett measurements; (○) Watanabe and Watanabe [32]; (▽) Biswas et al. [53]; (□) Blanke et al. [54].

the 333 K isotherm, the present $\rho(P, T)$ data fall within 0.07% of the data of Biswas et al. [31]. Notably, the present datum at 4.8 MPa agrees much better with the data of Biswas et al. than with the data of either Watanabe and Watanabe [32] or of Blanke et al. [33]. Thus, in a more complete correlation of the equation of state of SF_6, the present data may help resolve the discrepancies between these three, previously published sets of data.

ACKNOWLEDGMENT

This work was supported in part by the National Semiconductor Metrology Program.

REFERENCES

1. R. A. Aziz, M. J. Slaman, W. L. Taylor, and J. J. Hurly, *J. Chem. Phys.* **94**:1034 (1990).
2. N. Meinander, *J. Chem. Phys.* **99**:8654 (1993).
3. A. Oda, M. Uematsu, and K. Watanabe, *Bull. JSME* **26**:1590 (1983).
4. W. A. Cole and K. M. de Reuck, *Int. J. Thermophys.* **11**:189 (1990).
5. J. J. Hurly, *Int. J. Thermophys.* **20**:455 (1999).
6. K. A. Gillis, A. R. H. Goodwin, and M. R. Moldover, *Rev. Sci. Instrum.* **62**:2213 (1991).
7. K. A. Gillis, *Int. J. Thermophys.* **15**:821 (1994).
8. K. A. Gillis, *Int. J. Thermophys.* **18**:73 (1997).
9. J. J. Hurly, J. W. Schmidt, S. J. Boyes, and M. R. Moldover, *Int. J. Thermophys.* **18**:579 (1997).
10. L. A. Weber, *Int. J. Thermophys.* **10**:617 (1989).
11. D. E. Gray (ed.), *The American Institute of Physics Handbook*, 3rd ed. (McGraw–Hill, New York, 1972), pp. 4–126.
12. L. A. Weber, *J. Chem. Eng. Data* **41**:1477 (1996).
13. E. E. Totskii, Y. V. Karmyshin, and I. V. Talaev, *High Temp.* **22**:693 (1984).
14. L. A. Weber, *Int. J. Refrig.* **17**:117 (1994).
15. M. W. Chase, C. A. Davies, J. R. Downey, D. J. Frurip, R. A. McDonald, and A. N. Syverud, *J. Phys. Chem. Ref. Data* **14**:Suppl. No. 1 (1985).
16. G. E. Meyer and C. E. Buell, *J. Chem. Phys.* **16**:744 (1948).
17. J. Gaunt, *Trans. Faraday Soc.* **49**:1122 (1953).
18. T. E. Morsy, *Ber. Bunsenges. Phys. Chem.* **68**:277 (1964).
19. K. Bier, G. Maurer, and H. Sand, *Ber. Bunsenges. Phys. Chem.* **84**:430 (1980).
20. A. Eucken and A. Bertram, *Z. Phys. Chem.* **31**:361 (1936).
21. A. Eucken and H. Ahrens, *Z. Phys. Chem.* **26**:297 (1934).
22. J. P. M. Trusler, *Int. J. Thermophys.* **18**:635 (1997).
23. C. G. Maitland and E. B. Smith, *Chem. Phys. Lett.* **22**:443 (1973).
24. T. Kihara, *Rev. Mod. Phys.* **25**:831 (1953).
25. E. A. Mason and T. H. Spurling, *The Virial Equation of State* (Pergamon Press, Oxford, 1969).
26. R. J. Dulla, J. S. Rowlinson, and W. R. Smith, *Mol. Phys.* **21**:229 (1971).
27. B. M. Axilrod and E. J. Teller, *J. Chem. Phys.* **11**:299 (1943).
28. K. A. Gillis and M. R. Moldover, *Int. J. Thermophys.* **17**:1305 (1996).

29. A. Kumar, G. R. G. Fairley, and W. J. Meath, *J. Chem. Phys.* **83**:70 (1985).
30. J. J. Hurly, J. W. Schmidt, S. J. Boyes, and M. R. Moldover, *Int. J. Thermophys.* **18**:579 (1997).
31. S. N. Biswas, N. J. Trappeniers, and J. H. B. Hoogland, *Physica* **126A**:384 (1983).
32. K. Watanabe and H. Watanabe, *Proc. Seventh Symp. Thermophys. Prop.* (Am. Soc. Mech. Eng., New York, 1977).
33. W. Blanke, H. Häusler, and R. Weiss, *Int. J. Thermophys.* **9**:791 (1988).
34. A. K. Wyczalkowska and J. V. Sengers, submitted for publication.
35. V. P. Borisoglebskii, L. I. Strokovskii, and I. S. Zhiguleva, *Zh. Fiz. Khimii* **48**:1119 (1974).
36. V. A. Elema, *Teploenergetika* **17**:99 (1970).
37. S. A. Ulybin and E. P. Zherdev, *Sov. Phys. Doklady* **15**:306 (1970).
38. H. C. Miller, L. S. Verdelli, and J. F. Gall, *Ind. Eng. Chem.* **43**:1126 (1951).
39. W. C. Schumb and E. L. Gamble, *J. Am. Chem. Soc.* **52**:4302 (1930).
40. J. H. Dymond and E. B. Smith, *The Virial Coefficients of Pure Gases and Mixtures* (Clarendon Press, Oxford, 1980).
41. K. E. MacCormack and W. G. Schneider, *J. Chem. Phys.* **19**:845 (1953).
42. S. D. Hamann, W. J. McManamey, and J. F. Pearse, *Trans. Faraday Soc.* **49**:351 (1953).
43. H. P. Clegg and J. S. Rowlinson, *Trans. Faraday Soc.* **51**:1327 (1955).
44. W. H. Mears, E. Rosenthal, and J. V. Sinka, *J. Chem. Phys.* **73**:2254 (1969).
45. R. F. Hajjar and G. E. MacWood, *J. Chem. Eng. Data* **15**:3 (1970).
46. R. D. Nelson and R. H. Cole, *J. Chem. Phys.* **54**:4033 (1971).
47. Von J. Bellm, W. Reineke, K. Schäfer, and B. I. Schramm, *Ber. Bunsenges. Phys. Chem.* **78**:282 (1974).
48. P. M. Sigmund, I. H. Silberberg, and J. J. McKetta, *J. Chem. Eng. Data* **2**:168 (1972).
49. Von R. Hahn, K. Schäfer, and B. Schramm, *Bunsenges. Phys. Chem.* **78**:287 (1974).
50. C. Hosticka and T. K. Bose, *J. Chem. Phys.* **60**:1318 (1974).
51. J. Santafe, J. S. Urieta, and C. G. Losa, *Revta Acad. Cienc. Exact. Fis. Quim. Nat. Zaragoza* **31**:63 (1976).
52. J. Mollerup, *J. Chem. Eng. Data* **30**:21 (1985).
53. S. N. Biswas, N. J. Trappeniers, and J. H. B. Hoogland, *Physica* **126A**:384 (1983).
54. W. Blanke, H. Häusler, and R. Weiss, *Int. J. Thermophys.* **9**:791 (1988).